Aqueous Activated Graphene Dispersions for Deposition of High Surface Area Supercapacitor Electrodes

Vasyl Skrypnychuk,† Nicolas Boulanger,† Andreas Nordenström,† and Alexandr Talyzin†*

† Department of Physics, Umeå University, Umeå, SE-901 87, Sweden.

SUPPORTING INFORMATION

1. Preparation of arGO
2. Characterization of arGO precursor material: XPS, N2 sorption isotherms (SSA and pore size distribution), SEM.
3. Details of electrode preparation
4. Characterization of coated electrodes using Raman spectroscopy, XRD, TGA, optical microscopy.

5. Details of characterization methods and calculations.

6. Additional data for electrochemical characterization of supercapacitor devices.

7. Additional information about rheological properties and stability of dispersions.

1. Preparation of aRGO

Reduced graphene oxide (RGO) and graphene oxide (GO) powders were purchased from Abalonyx (Norway), nanocrystalline fumed silica was purchased from Sigma-Aldrich. We are grateful to OCSiAl for providing a sample of single walled carbon nanotubes (SWCNT) used in this study.

Thermal activation of reduced graphene oxide was performed using slightly modified KOH activation procedure optimized for high BET surface area.[1-2] RGO was mixed with KOH (1:8 wt) dissolved in water:ethanol (3:7 wt) mixture, followed by drying in vacuum oven. The sample was heated under argon flow up to the target temperature of 850^{o}C for 140 min, followed by 40 min annealing at this target temperature and cooled down to room temperature. The obtained reaction product was washed with 10% aqueous solution of acetic acid, filtered using a PTFE filter, washed with water and dried.

2. Characterization of arGO.

Detailed characterization of GO precursor material and arGO materials prepared at different conditions was performed in our earlier study.[3] Commercial Abalonyx graphite oxide, prepared by the modified Hummers method with C/O = 1.99 and 0.94 at.% of sulphur impurity (determined by XPS) was used as the precursor. Excluding oxygen added to the material as a sulphate the C/O ratio is corrected to 2.3. The graphite oxide was subjected to rapid explosive thermal exfoliation by inserting it into hot furnace (235°C) for 2 min. The powder rGO was then used to prepare high surface area a-rGO.[2, 4]

The a-rGO material showed no diffraction peaks in XRD and low oxygen content (C/O=55 determined by comparing areas of C1s and O1s) according to XPS, Figure S1.

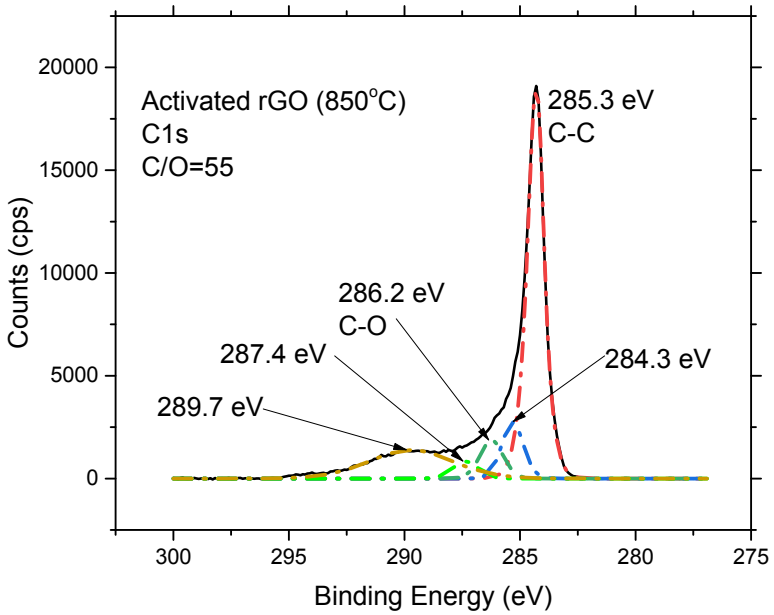

Figure S1. XPS spectrum of arGO powder sample (C1s).

Specific Surface Area (SSA) determined using analysis of nitrogen sorption isotherms shows some batch-to-batch variation. The arGO batch used for preparation of electrodes in this study showed Specific Surface Area (SSA) of ~2580 m^2/g by BET and ~2150 m^2/g using QSDFT model (Figure S2). The analysis of the nitrogen sorption isotherm using QSDFT slit pore model shows that almost 100% of pore volume is in pores with diameter below 4 nm.

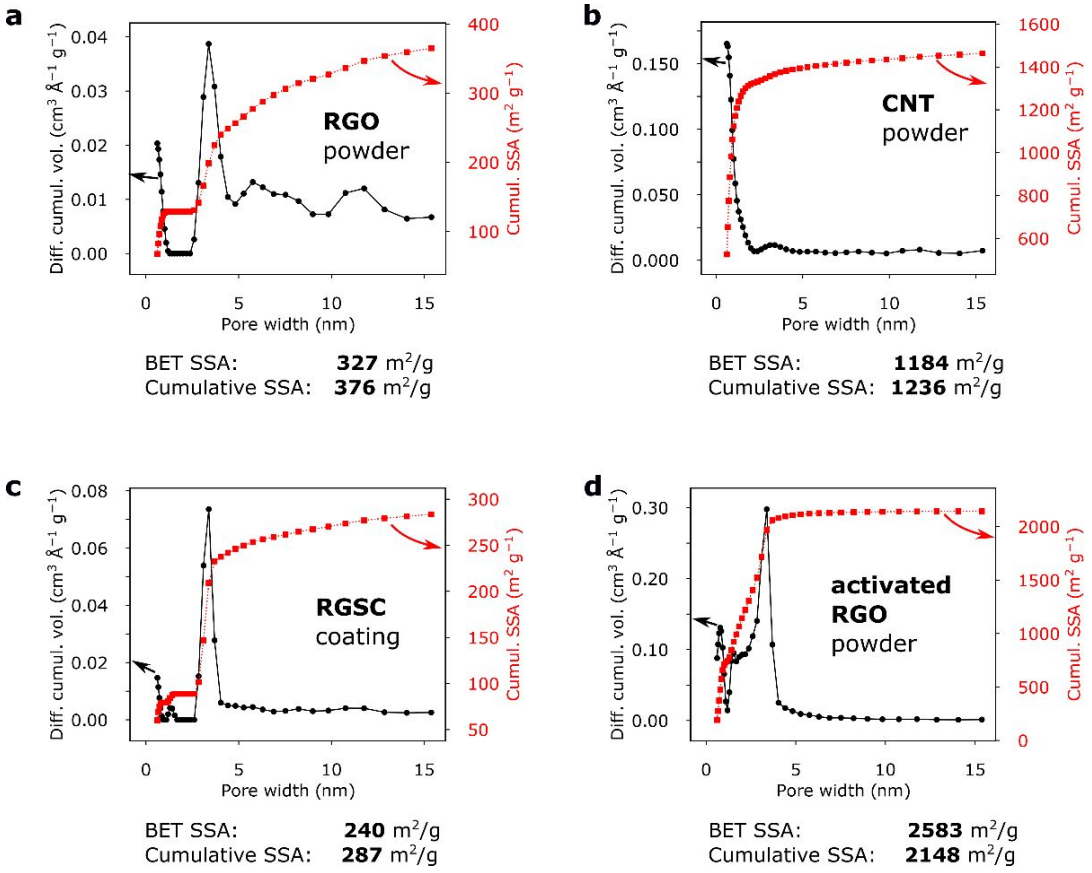

Figure S2. Analysis of nitrogen adsorption isotherms using the QSDFT slit pore model: cumulative pore distribution (red curve, right axis) and pore size distribution (black curve, left axis). (a) initial RGO powder; (b) initial CNT powder; (c) coated dispersion based on RGO, GO, fumed silica and CNT; (d) initial powder of KOH-activated RGO. The BET and cumulative specific surface area values are listed under the plots.

Porous structure of a-rGO was also confirmed using direct microscopic characterization using SEM (Figure S3) and STEM.[3]

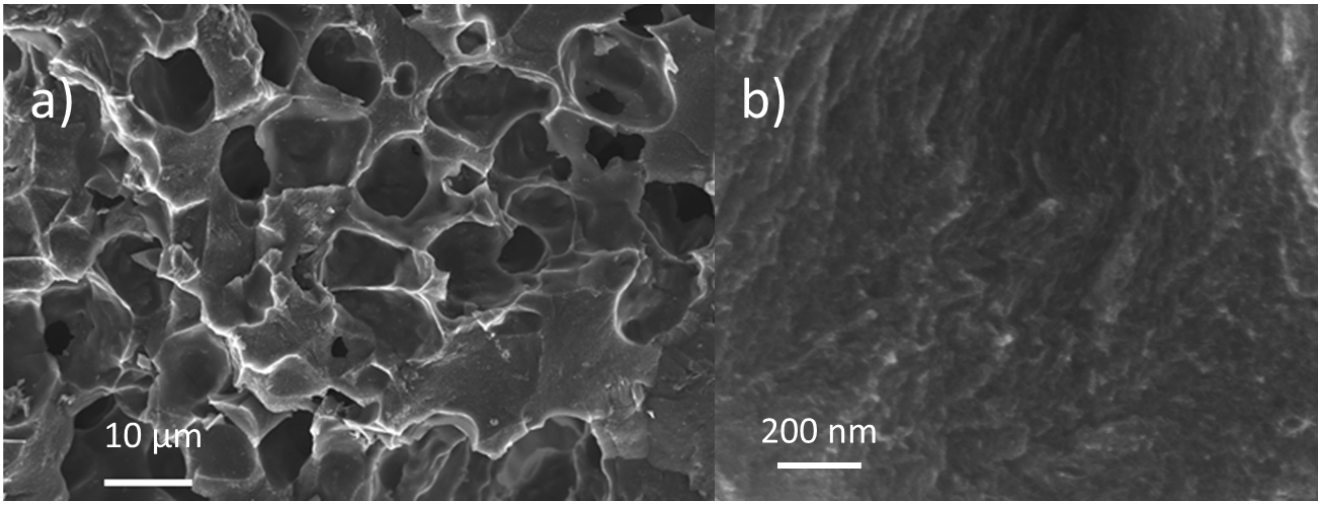

Figure S3 SEM images recorded using typical sample of a-rGO a) low magnification image of as-prepared a-rGO with micrometer sized cavities; b) high resolution image showing traces of layered structure inherited from rGO and observed even after activation. Nanometer sized pores were also imaged from similar a-rGO samples using STEM in our earlier publication. .[3]

Hydrophobic nature of a-rGO was confirmed also using Dynamic Vapor Sorption (DVS) method. The sample of a-rGO similar to the used here for preparation of electrodes showed almost negligible BET SSA value of ~8 m^2/g by water sorption. However, relatively large pore volume of 0.87 $cm^3\ g^{-1}$ was measured using full isotherm which exhibit the shape which points out to condensation of water inside the pores at P/P_0 above ~0.7.[3]

3. Preparation of dispersions and electrodes.

The aqueous dispersions were prepared using sequential mixing of the components using Mixed Mill MM400 vibrational ball milling machine (RetschVolume) equipped with an agate cell. The oscillation frequency of 30 s^{-1} was used for 5 minutes for each mixing

step. First, low surface area components (graphene oxide, fumed silica) were mixed with the aqueous dispersion medium and then mixed with carbon nanotubes. Finally, the rGO-based component (either rGO or activated rGO, depending on the formulation) was added and mixed. The optimized component weight ratio of 10:1:1:1 (a-rGO : GO : SiO_2 : CNT) was used for experiments as described in the main section. Typical concentration used for deposition of electrodes was 20 mg/ml counting only a-rGO or 26 mg/ml counting all components. The aqueous dispersions were coated onto flexible stainless steel foils using manual doctor blade coating technique, followed by drying at ambient conditions. After drying, part of the electrode was scraped off the steel foil, dried in a vacuum oven and analyzed by nitrogen adsorption in order to estimate the actual surface area of the coated electrode. The thickness of electrodes tested in supercapacitors was 100-500 μm. Typical samples were prepared using 2.13-2.21 mg/cm^2 loading. The weight of electrodes was measured after vacuum degassing at 130^{0}C.

4. Additional characterization of electrodes prepared using rGO and arGO dispersions.

4.1 Raman spectra

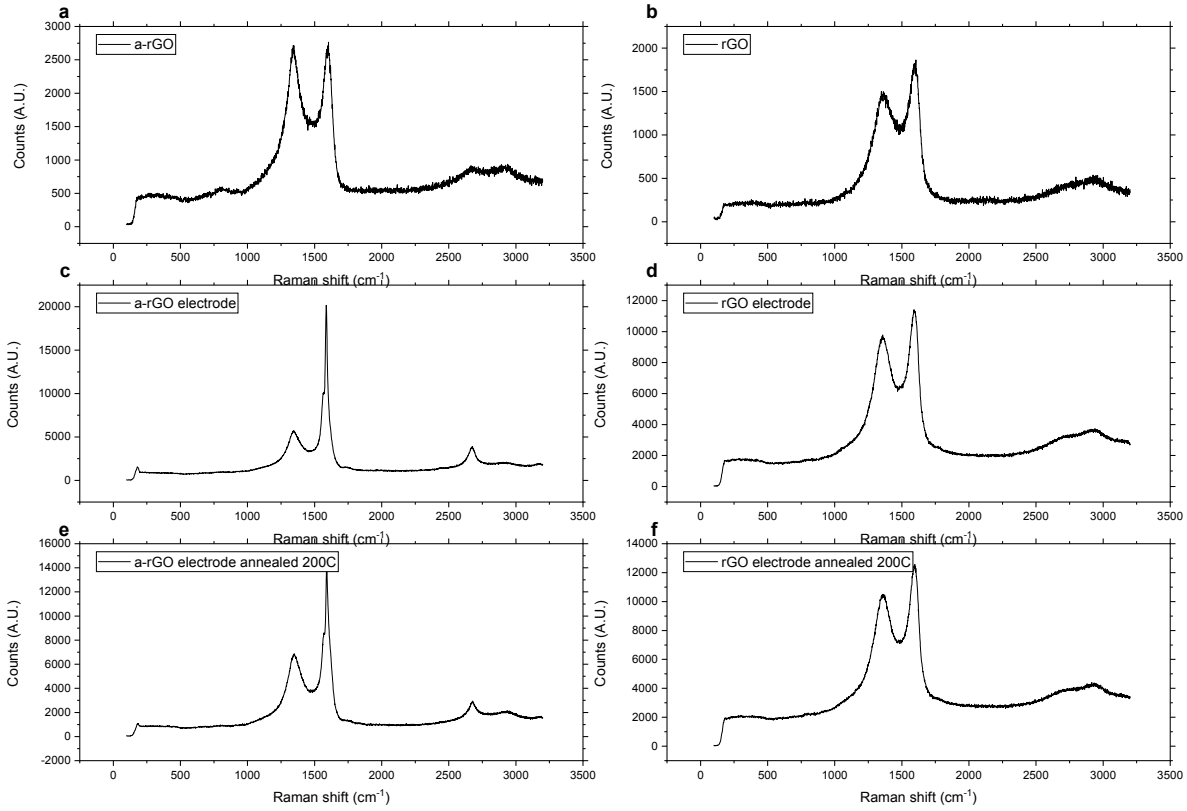

Figure S4. Raman spectra recorded from precursor a-rGO and reference rGO (a and b respectively), spectra of a-rGO and rGO electrode coated using dispersions (c and d respectively) and spectra of coated a-rGO and reference rGO electrodes annealed at 200^0C (e and f).

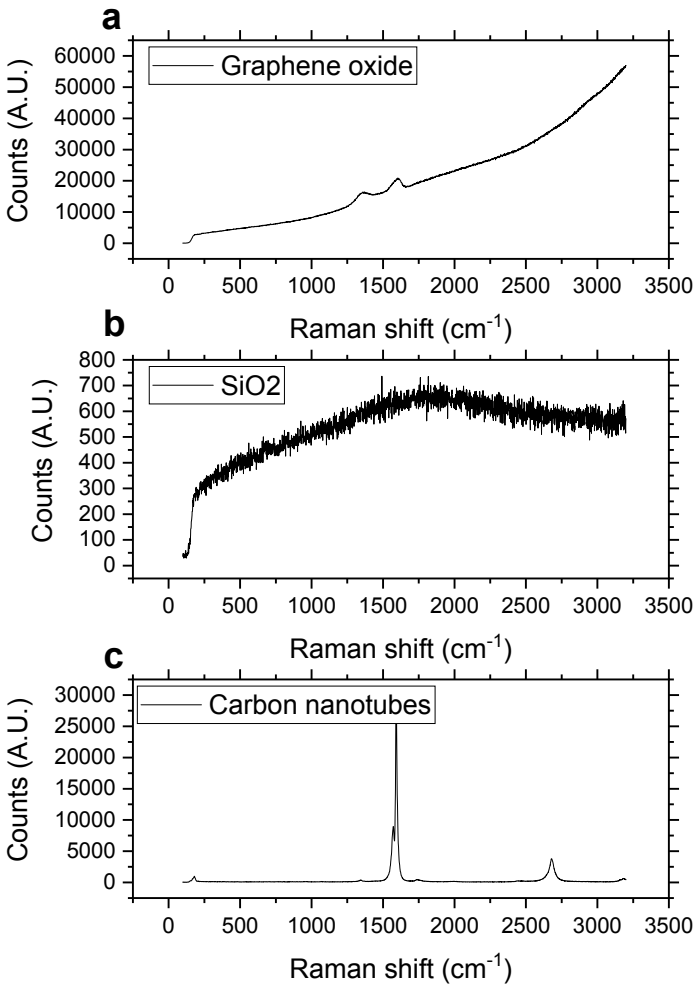

Figure S5 Raman spectra of precursor materials used for preparation of dispersions: a) graphene oxide, b) SiO2 and c) Carbon nanotubes

4.2 X-ray diffraction characterization of coated electrodes.

All materials used for preparation of electrodes are poorly crystalline and strongly disordered. Therefore, XRD do not provide significantly important information about the structure of electrodes. XRD patterns of coated electrodes is mostly a sum of XRD from all components. Ball milling used for preparation of dispersions provides additional disorder. As a result XRD of a-rGO electrodes exhibits one broad and asymmetric peak centered at ~5.9 degrees (d-spacing 14.98 Å) and small peak from graphitic d(002)=3.35Å, both are likely originate from mechanically deformed CNT's bundles (d(100)=16.99Å in the pattern of precursor CNT, Figure S7). Precursor a-rGO shows only one weak XRD reflection with d=2.08Å (due to in plane graphene lattice) and strong diffuse scattering at low angles is due to disordered structure of porous sample.

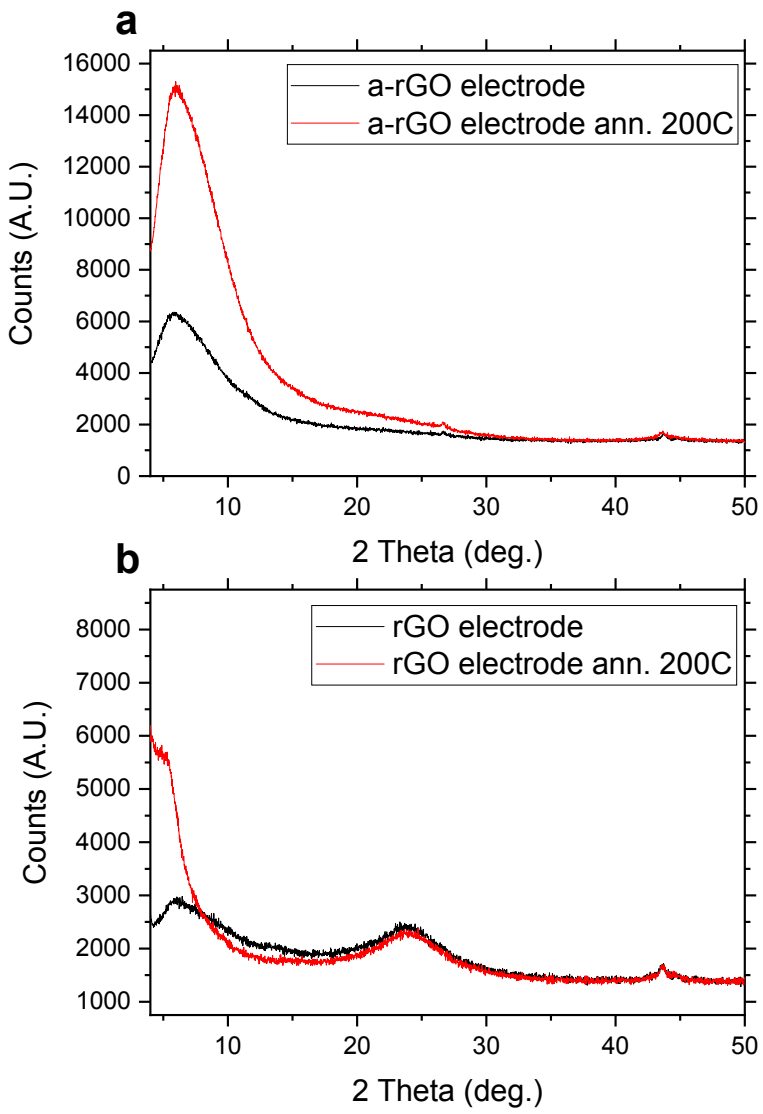

Figure S6. XRD patterns recorded form coated a-rGO based and rGO based electrodes. CuKα radiation.

Nearly amorphous structure of a-rGO is expected for the material composed by defect graphene sheets assembled in disordered 3D network. Precursor graphite oxide shows relatively strong but broad (001) reflection. Dispersing graphite oxide provides graphene

oxide in solution. Re-stacking of graphene oxide after electrode coating is not significant as evidenced by absence of (001) peak, as it is expected considering relatively low amount of GO relative to other components.. Annealing at 200^0C do not result in significant change of XRD patterns for both a-rGO and rGO based electrodes confirming absence of crystalline GO in the not heated samples.

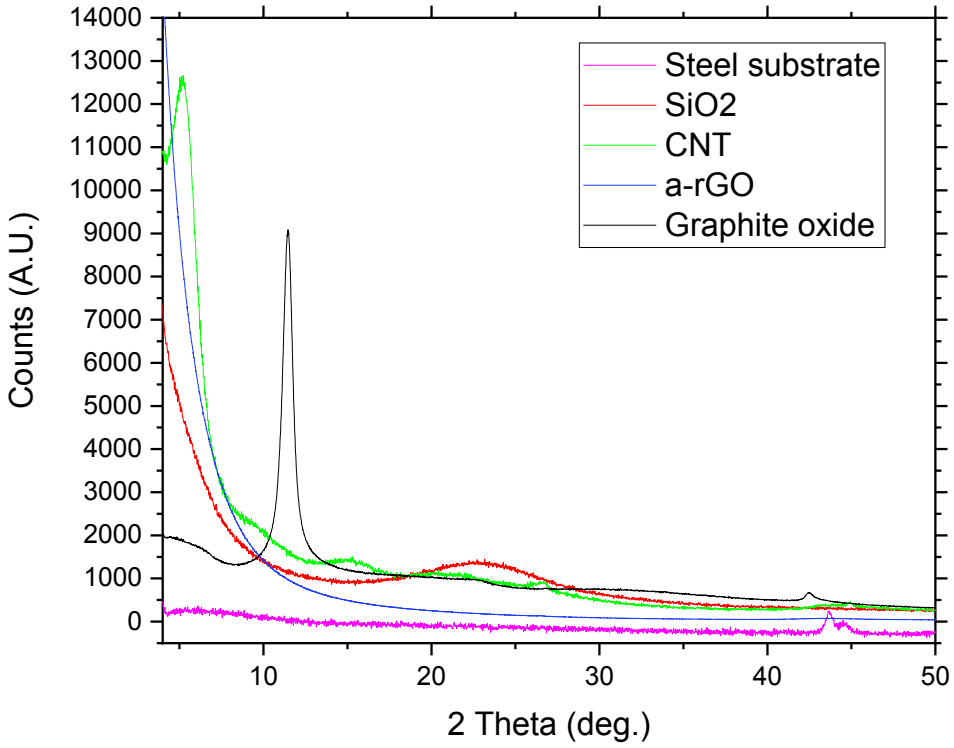

Figure S7 XRD patterns of precursor SiO2, CNT's and steel substrate. CuKα radiation.

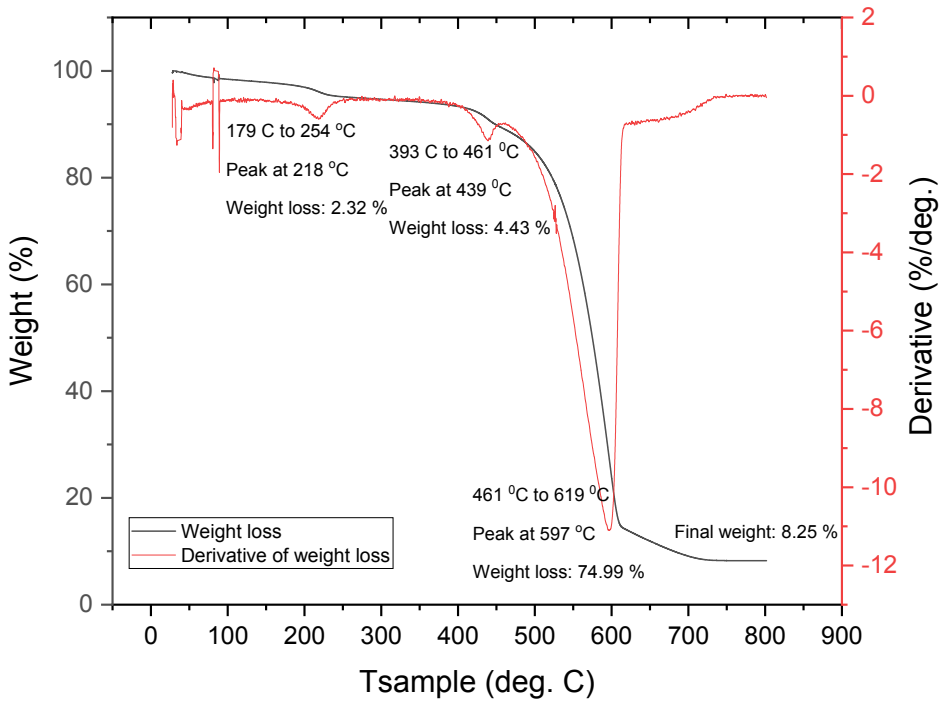

Figure S8. TGA data for a-rGO based electrode material recorded in air with 3deg/min rate.

The TGA provide insight into the composition of a-rGO- based electrodes. The first weight loss (2.3%) step corresponds to thermal deoxygenation of GO. Complete oxidation and removal of carbon result sin 8.25% residual mostly due to SiO2.

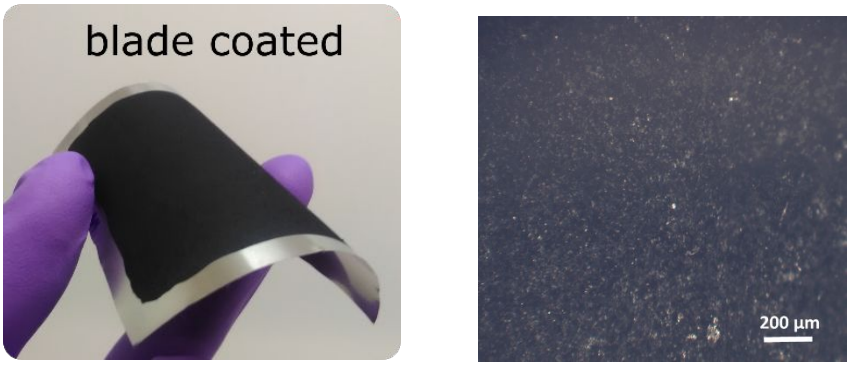

Figure S9 a) Image of a-rGO based electrode coated on stainless steel current collector; b) optical microscopy image of a-rGO electrode surface take with 20×objective

5. Methods

The BET specific surface area was evaluated by analysis of nitrogen sorption isotherms acquired using Autosorb iQ XR analyzer by Quantachrome. A slit pore quenched solid density functional theory (QSDFT) equilibrium model was used to evaluate cumulative

SSA, pore volume and pore size distribution of the samples. SEM images were recorded using a Zeiss Merlin FEG-SEM microscope.

Electrochemical characterization of electrodes prepared using dispersions was performed using Autolab PGSTAT204 potentiostat/galvanostat. Measurements were performed using standard two-electrode cell in aqueous (6M KOH) and organic (1M TEA BF_4 in acetonitrile). For each measurement, two square electrodes of approx. 1 cm^2 area were cut out of the electrode-coated steel foil, dried in an oven and weighed. Mass of the coating per unit mass of the steel foil was measured by scraping off and weighing a sample of the dried coating and used for the estimation of the weight of the electrode coating. Glass fiber membranes (Whatman GF/A) were used as separators for the aqueous electrolyte cells, plastic porous membranes (Celgard 3501) were used as separators for the supercapacitor cells based on organic electrolyte. CV curves were measured in the voltage range 0-1 V (aqueous electrolyte) or 0-2.7 V (organic electrolyte) at the scan rates of 50, 100, 200 and 500 mV/s. Charge-discharge curves were measured in the voltage range 0-1.0 V (aqueous electrolyte) and 0-2.7 V (organic electrolyte) at specific current values of 0.5, 1, 2, 3, 5, 10, 20 and 40 A/g. Specific capacitance, energy

density and power density were estimated based on the galvanostatic discharge data using the standard procedure reported in the literature.[5-7]

Specific capacitance, energy density and power density calculations.

Specific capacitance of a single electrode $C_{el,sp}$, the energy density of the whole electrode stack E and the power density P for two electrode cell were calculated using procedure described below.

Table 1 List of symbols used in the calculations and their description.

Symbol	Description
U_r	Maximum voltage reached during charging (V)
U_{max}	Starting voltage of the discharge after the drop due to the equivalent distributed resistance (V)
U_{min}	Final voltage at the end of the discharge (V)
ΔU	$U_{max} - U_{min}$ (V)
I	Applied current (A)

EDR	Equivalent distributed resistance (**Ω**)
Q	Charge (**C**)
T_{start}	Starting time of the discharge (**s**)
T_{end}	End time of the discharge (**s**)
Δt	$T_{end} - T_{start}$ (**s**)
C_{2el}	Capacitance of the whole stack of electrodes (**F**)
$C_{2el,sp}$	Specific capacitance of the whole stack of electrodes (**F/g**)
C_{el}	Capacitance of a single electrode (**F**)
$C_{el,sp}$	Specific capacitance of a single electrode (**F/g**)
M	Total mass of the electrode stack (**g**)
m	Mass of a single electrode (**g**)
E	Energy density of the electrode stack (**Wh/kg**)
P	Power density of the electrode stack (**W/kg**)

Specific capacitance:

The capacitance was determined from galvanostatic constant current charge/discharge (CCCD) curves measured at different current densities. For each curve, the discharge was integrated after the voltage drop due to the equivalent distributed resistance (EDR), meaning that while the charge of the capacitor goes to U_r the discharge starts at $U_{max} = U_r - I * EDR$ where I is the applied current.

Such a curve for a 1A/g charge/discharge is shown Figure 1 for a capacitor using activated reduced graphene oxide as electrode material in 6M KOH.

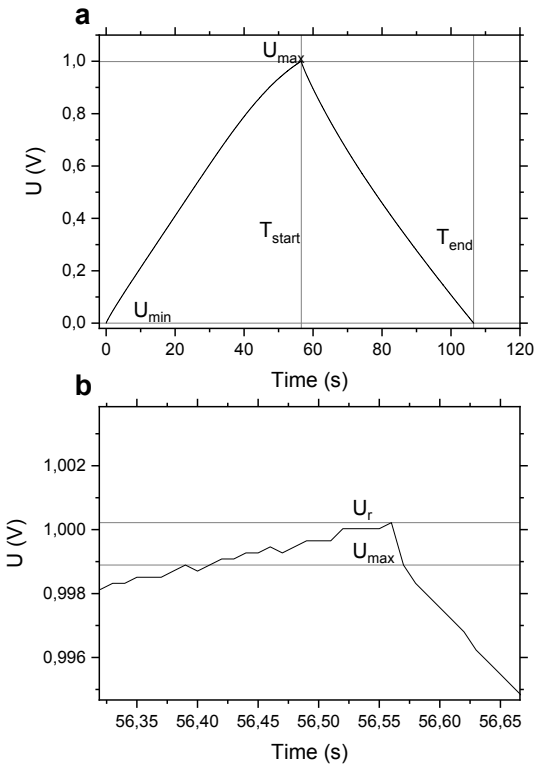

Figure S10 Charge discharge curved for the activated reduced graphene oxide capacitor at 1A/g in 1M KOH. a) shows the full curve while b) focuses on the voltage drop at the beginning of the discharge.

Linear profile:

In the case of a linear discharge profile, the capacitance of the electrodes stack C_{2el} can be determined as $C_{2el} = \frac{Q}{\Delta U} = \frac{I\,\Delta t}{\Delta U}$ where Q is the charge, ΔU the measured voltage drop

due to the discharge ($U_{max} - U_{min}$), I is the applied current in A and Δt is the time elapsed during the discharge ($T_{end} - T_{start}$).

On the example given Figure S10, the discharge takes place between 0.999 V and 3.96 10^{-5} V during 50.0 s for a current density of 1 A/g. The electrode stack weighed 2.10 mg, meaning the applied current was 0.00210 A, resulting in a capacitance of 0.105 F.

The capacitance obtained this way is the total capacitance of the double layer capacitor used for the measurement. Both electrodes have a similar weight, therefore it is assumed that C_{el1} and C_{el2} the capacitances of each electrodes are equal. As they are connected in series in the device, the capacitance can be written as:

$$C_{2el} = \frac{C_{el1} * C_{el2}}{C_{el1} + C_{el2}} \#(1)$$

Here $C_{el1} = C_{el2}$ therefore $C_{2el} = \frac{{C_{el}}^2}{2 * C_{el}}$ resulting in capacitance for one electrode:

$$C_{el} = 2 * C_{2el} \#(2)$$

Specific capacitance is calculated by normalizing experimentally measured capacitance to the electrode weight. Here the total amount M of electrode material (without considering

the steel supports) was 2.10 mg, meaning the mass of one electrode m was 1.05 mg. In the given example, the resulting specific capacitance of the electrode is therefore **200 F/g**.

In practical applications, only the first part of the discharge (until $\frac{U_{max}}{2}$) is considered. In this case, the discharge time is also shorter. For the electrode shown Figure 1, this means a voltage drop from 0.999 V until 0.499 V in 21.3 s, resulting in a capacitance for both electrode of 0.090 F and therefore a specific capacitance for a single electrode of **170.4 F/g**.

Non-linear profile:

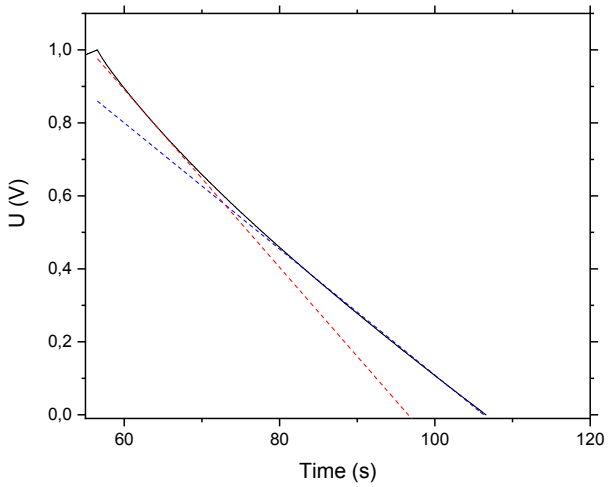

Figure S11 Discharge curve of the capacitor from Figure 1 with linear fit of the first part of the discharge (red) and the second part of the discharge (blue), showing non linearity of the discharge process.

However, as highlighted in Figure 2, the capacitor discharge curve is not linear. Therefore, in order to increase the accuracy of the measurement, the integration of the discharge curve was used instead, leading to:

$$C_{2el} = 2 * I * \frac{\int U dt}{\left(U_{max}^2 - U_{min}^2\right)} \#(3)$$

The integration of the discharge curve from Figure 1 gives a value of 22.472 Vs, resulting in a capacitance for the stack of 0.095 F. Calculating the value for one electrode using equation 2 therefore gives a specific capacitance of **180 F/g**.

When considering a discharge until only $\frac{U_{max}}{2}$, the integration of the partial discharge curve gives a value of 15.507 Vs, resulting in a capacitance for the stack of 0.087 F, meaning the specific capacitance for the single electrode is **165 F/g**.

Energy density and power density:

The energy density E of the supercapacitor can be determined for each charge/discharge as:

$$E = \frac{1}{M} I \int_{U_{min}}^{U_{max}} U(t)dt = \frac{1}{M} \frac{1}{2} C_{2el}\left((U_r - I * EDR)^2 - U_{min}^2\right) = \frac{1}{M} \frac{1}{2} C_{2el}\left(U_{max}^2 - U_{min}^2\right) \#(4)$$

where EDR is the equivalent distributed resistance and M is the mass of the electrode stack (here the total mass of the active material of both electrodes). When considering only the first half of the discharge, this equation then becomes

$$E = \frac{1}{M} \frac{1}{2} C_{2el}\left(U_{max}^2 - \left(\frac{U_{max}}{2}\right)^2\right) = \frac{1}{M} \frac{3}{8} C_{2el}\, U_{max}^2 \#(5)$$

It should be noted that in equations (4) and (5), the specific capacitance $C_{2el,sp}$ can be used instead, removing the need to divide by the total mass M.

When standard units are used, the energy density will be in J/g. Reported values are usually in Wh/kg, therefore the energy density needs to be divided by 3.6 in order to convert it to Wh/kg from J/g.

For the electrode shown Figure 1, this results in an energy density of 25 J/g (**6.94 Wh/kg**) using a specific capacitance of 200 F/g when considering a linear profile or, when considering the first half of the discharge (specific capacitance of 170 F/g) an energy density of 16.0 J/g (**4.43 Wh/kg**).

When considering integration method, the obtained specific capacitance of 180 F/g results in an energy density of 22.5 J/g (**6.24 Wh/kg**). For the figures presented in this paper we used values obtained by integration method and full discharge curve.

The power density P in W/kg is then derived from the energy density E in Wh/kg using:

$$P = \frac{E}{\Delta t} * 3600 \#(6)$$

where Δt is the discharge time in seconds. For the example shown above, this results in **499 W/kg** when considering a linear profile or, for integration method, **449 W/kg**.

6. Additional data for electrochemical characterization of supercapacitor devices.

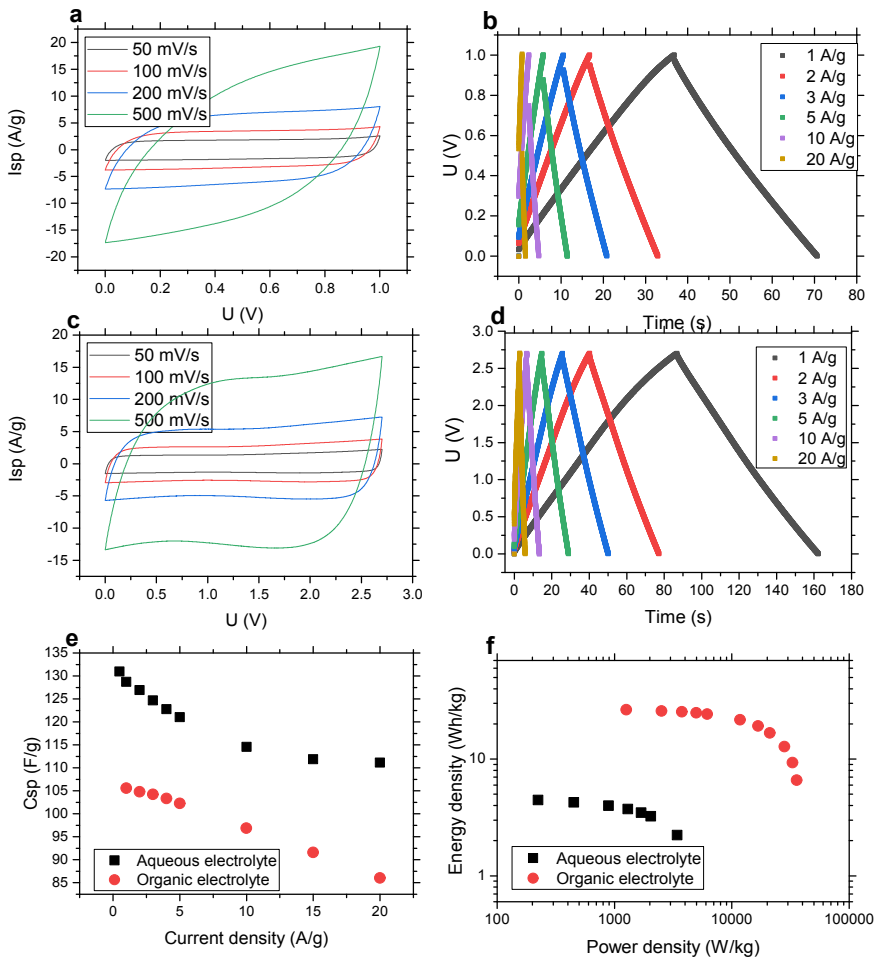

Figure S12. Electrochemical characterization of a-rGO based electrodes deposited at ambient temperature and dried without additional annealing. CV curves and galvanostatic charge discharge a,b- in 6M KOH electrolyte, c,d- organic electrolyte; e)- gravimetric capacitance, d) Ragone plot.

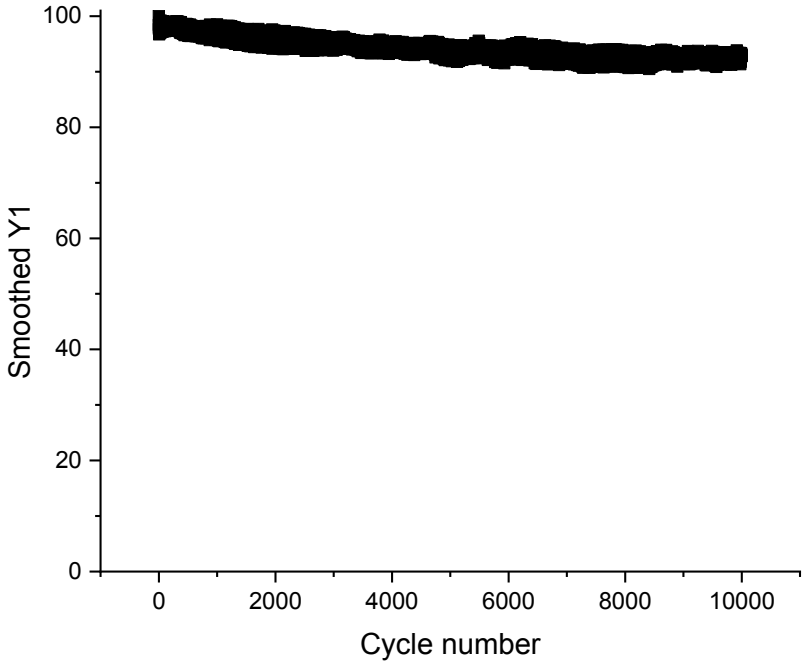

Figure S13. Cycling stability of the a-RGO-based coated electrodes in 6M KOH electrolyte. Capacitance retention of 93.% was observed in this experiment after 10000 galvanostatic charge-discharge cycles at current density of 0.5 A/g

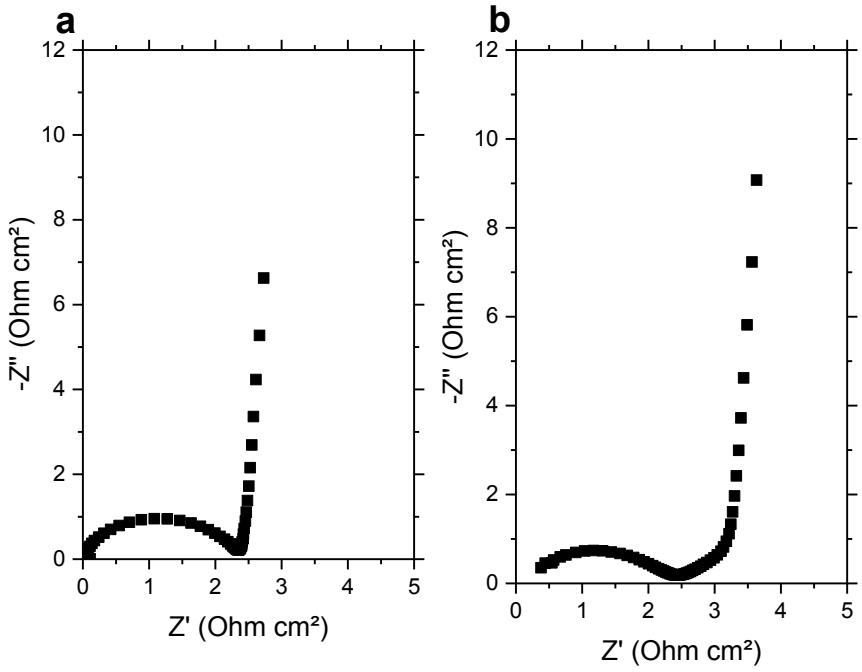

Figure S14. Nyquist plots of the symmetrical supercapacitors based on the dispersion-coated high SA a-RGO electrodes. Tested in (a) 6M KOH electrolyte; (b) 1M TEA BF_4 in acetonitrile electrolyte. Frequency range: 0.1-100000 Hz.

Detailed for analysis of Nyquist plots was recently reviewed by B.A.Mei et al[8] citing some significant differences in interpretation of physical meaning for main features of complex impedance plots. The data shown in Figure S10 demonstrate that electrodes studied in acetonitrile electrolyte exhibit slightly higher diameter of semicircle (most commonly assigned to internal resistance) , broader non vertical part related to ion transport

limitations (larger equivalent distribution resistance, EDR) and almost the same slope for linear part at lower frequencies (as compared to aqueous electrolyte).

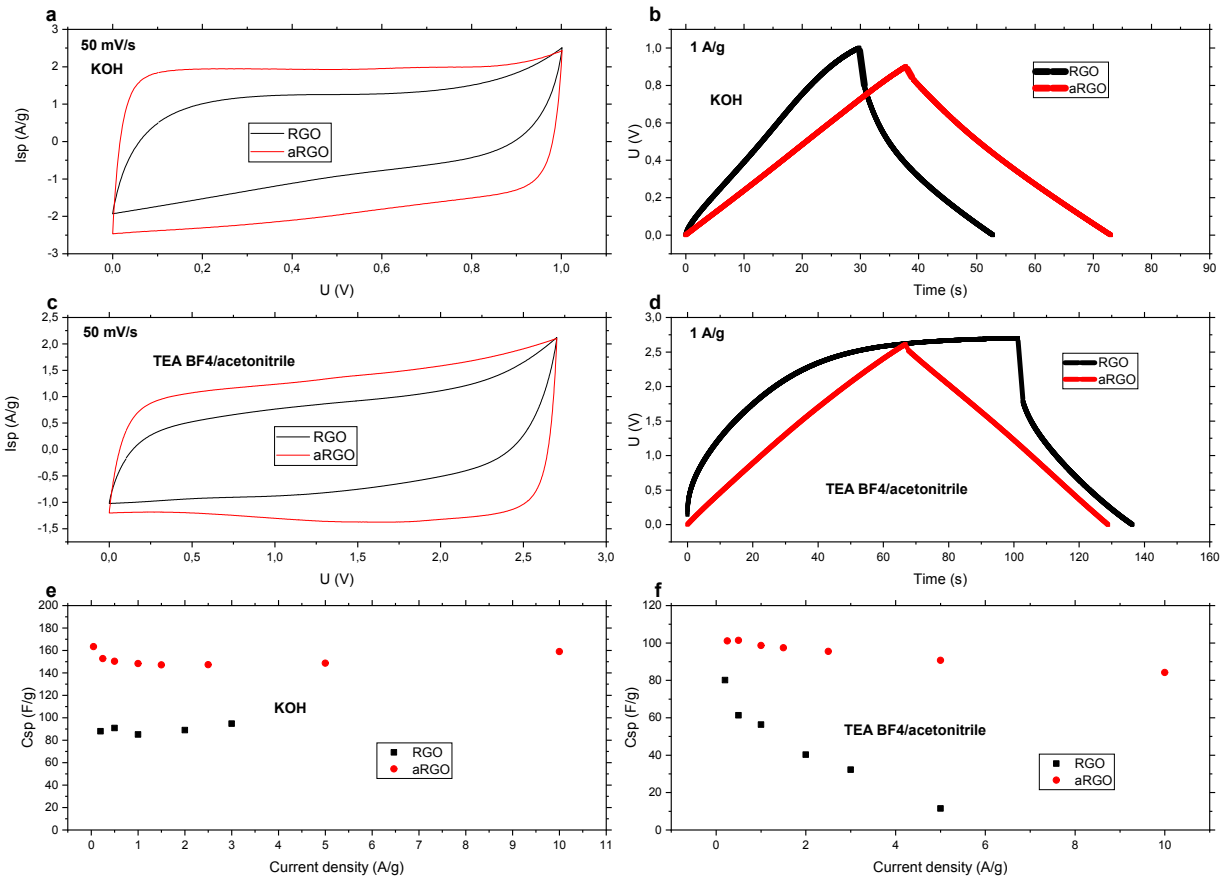

Figure S15. Electrochemical characterization of electrodes prepared using aqueous dispersions based on (a-rGO) and rGO (both with no post-deposition annealing) and tested in two electrode cell with aqueous electrolyte (6M KOH) (a,b,e) and organic electrolyte (c,d,f). (a,c) CV curves at the scanning rate of 50 mV/s; (b,d) galvanostatic charge-discharge curves at the current density of 1 A/g; note the much shorter discharge times and significantly higher voltage drop measured for the RGO-based electrodes; (e,f) specific capacitance vs current density, calculated using the galvanostatic discharge data. Mechanical decomposition of the rGO-based electrodes was observed at higher current densities.

7. Additional information about rheological properties and stability of dispersions.

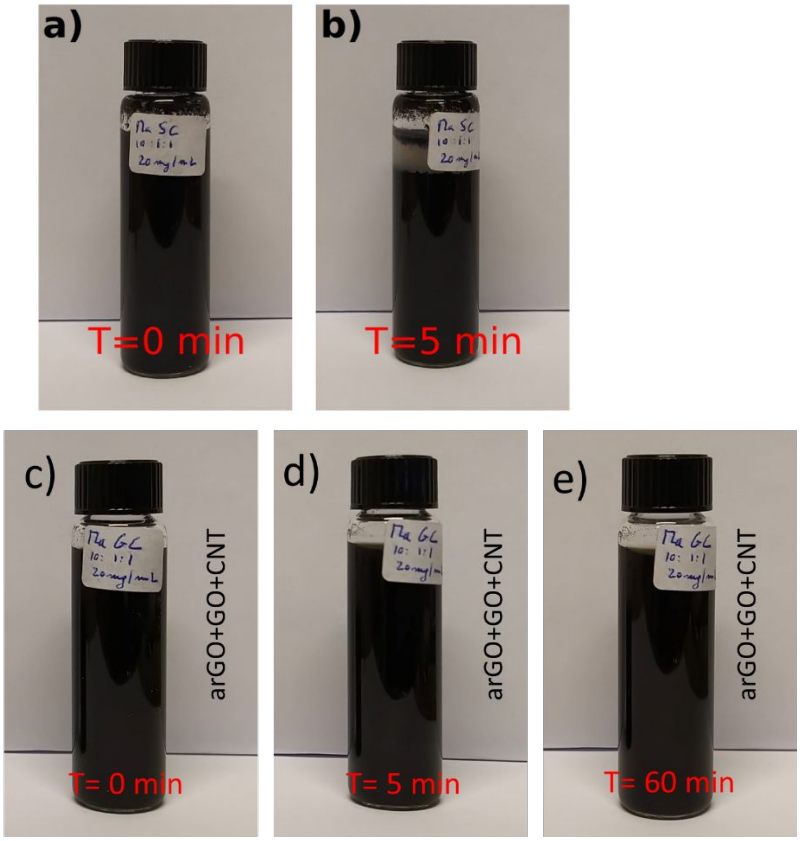

Figure S16. The dispersions prepared without GO (arGO:SiO_2:CNT= 10:1:1) are not stable and some precipitation is observed already after 5 minutes (a, b). In contrast, dispersions prepared using GO (arGO:GO:CNT=10:1:1) are more stable even without addition of SiO_2 (c,d,e). Some precipitation on the bottom of the vial was observed only after several hours of storage.

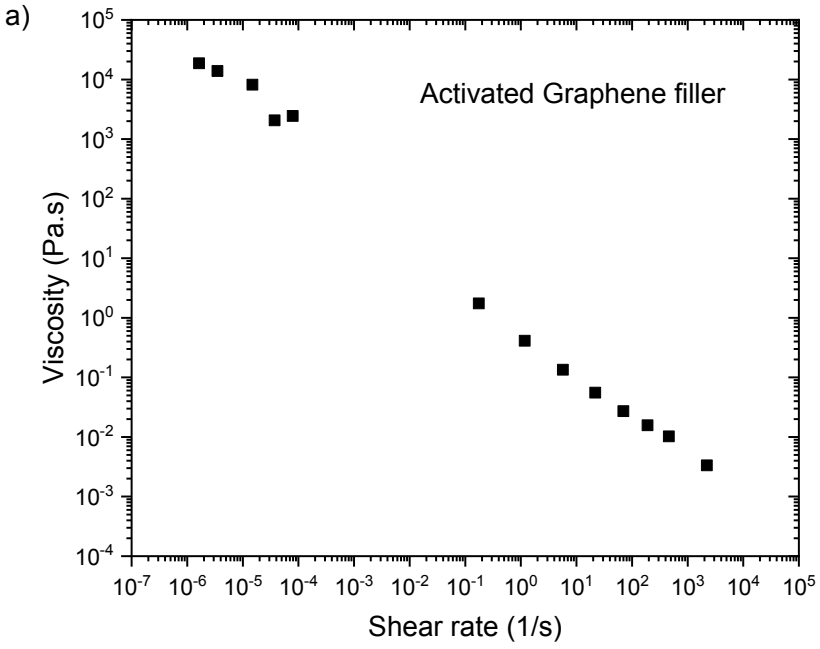

Figure S17. Shear rate vs viscosity plots for 20 mg/ml dispersions prepared using arGO filler.

Stress sweep rheological measurements were done to investigate the viscoelastic properties of the concentrated rGO and arGO dispersions on a TA Instruments DHR-2 rheometer equipped with a Peltier plate for temperature control. A parallel plate geometry (8 mm) was used for all

experiments. All samples were tested for a linear viscoelastic region between 0.05 and 100 μNm, using torque sweep at a constant frequency of 0.2 Hz.

The dispersions based on arGO and AC fillers show qualitatively similar plots except for low shear rates values where rGO showed small flat region. The dispersions are non-Newtonian exhibiting shear-thinning behavior. The data shown in Figure S13 are similar to the properties of concentrated aqueous GO dispersions.[9-10] Detailed study of rheological properties of the dispersions as a function of relative amounts of components and concentration is outside of scope of our study. It should be noted that rheological properties of GO dispersions with rGO and CNT's as fillers were not reported in previously published studies mostly focused on properties of materials prepared by the ink/dispersion drying.[11-12]

Supplementary References

1. Zhu, Y. W., et al., Carbon-Based Supercapacitors Produced by Activation of Graphene. *Science* 2011, *332*, 1537-1541.

2. Klechikov, A.; Mercier, G.; Sharifi, T.; Baburin, I. A.; Seifert, G.; Talyzin, A. V., Hydrogen Storage in High Surface Area Graphene Scaffolds. *Chem Commun* **2015**, *51*, 15280-15283.
3. Iakunkov, A.; Skrypnychuk, V.; Nordenstrom, A.; Shilayeva, E. A.; Korobov, M.; Prodana, M.; Enachescu, M.; Larsson, S. H.; Talyzin, A. V., Activated Graphene as a Material for Supercapacitor Electrodes: Effects of Surface Area, Pore Size Distribution and Hydrophilicity. *Phys Chem Chem Phys* **2019**, *21*, 17901-17912.
4. Klechikov, A. G.; Mercier, G.; Merino, P.; Blanco, S.; Merino, C.; Talyzin, A. V., Hydrogen Storage in Bulk Graphene-Related Materials. *Micropor Mesopor Mat* **2015**, *210*, 46-51.
5. Kim, T.; Jung, G.; Yoo, S.; Suh, K. S.; Ruoff, R. S., Activated Graphene-Based Carbons as Supercapacitor Electrodes with Macro- and Mesopores. *Acs Nano* **2013**, *7*, 6899-6905.
6. Stoller, M. D.; Ruoff, R. S., Best Practice Methods for Determining an Electrode Material's Performance for Ultracapacitors. *Energ Environ Sci* **2010**, *3*, 1294-1301.
7. Rodriguez-Martinez, L., *Emerging Nanotechnologies in Rechargeable Energy Storage Systems*; Elsevier: Boston, MA, 2017, p pages cm.
8. Mei, B. A.; Munteshari, O.; Lau, J.; Dunn, B.; Pilon, L., Physical Interpretations of Nyquist Plots for Edlc Electrodes and Devices. *J Phys Chem C* **2018**, *122*, 194-206.
9. Valles, C.; Young, R. J.; Lomax, D. J.; Kinloch, I. A., The Rheological Behaviour of Concentrated Dispersions of Graphene Oxide. *J Mater Sci* **2014**, *49*, 6311-6320.
10. Del Giudice, F.; Shen, A. Q., Shear Rheology of Graphene Oxide Dispersions. *Curr Opin Chem Eng* **2017**, *16*, 23-30.
11. Yu, D. S.; Dai, L. M., Self-Assembled Graphene/Carbon Nanotube Hybrid Films for Supercapacitors. *J Phys Chem Lett* **2010**, *1*, 467-470.
12. Guo, S. R.; Wang, W.; Ozkan, C. S.; Ozkan, M., Assembled Graphene Oxide and Single-Walled Carbon Nanotube Ink for Stable Supercapacitors. *J Mater Res* **2013**, *28*, 918-926.